Petroleum Science 21 (2024) 3965–3980

Contents lists available at ScienceDirect

Petroleum Science

journal homepage: www.keaipublishing.com/en/journals/petroleum-science

Original Paper

Rock physics properties and influencing factors of subsalt carbonate reservoir of Ordovician Majiagou Formation in central Ordos Basin

Jia-Qing Wang [a, b], Ji-Xin Deng [a, b, *], Zhong-Hua Xu [c, d], Hui Xia [a, b], Long-long Yan [a, b]

[a] Key Laboratory of Earth Exploration & Information Technology, Ministry of Education, Chengdu University of Technology, Chengdu, 610059, Sichuan, China
[b] College of Geophysics, Chengdu University of Technology, Chengdu, 610059, Sichuan, China
[c] PetroChina Research Institute of Petroleum Exploration & Development-Northwest, Lanzhou, 730000, Gansu, China
[d] Key Laboratory of Petroleum Resources of CNPC, Lanzhou, 730000, Gansu, China

ARTICLE INFO

Article history:
Received 3 January 2024
Received in revised form
23 April 2024
Accepted 28 May 2024
Available online 29 May 2024

Edited by Meng-Jiao Zhou

Keywords:
Rock physics properties
Carbonate rock
Sedimentary environment
Ordovician majiagou formation
Ordos basin

ABSTRACT

The carbonate reservoirs in the Ordovician Majiagou Formation of the Ordos Basin have undergone complex geological evolution, resulting in high-quality dolomite reservoirs that exhibit strong heterogeneity. Neglecting the fundamental factor of reservoir genetic mode, conventional rock physics experiments cannot accurately determine the seismic elastic responses of the target rock. Here, a set of carbonate samples from different sedimentary environments were selected elaborately based on geological and logging data. Subsequently, systematic petrological and rock physics measurements were conducted to investigate the variation of rock physics properties from both macro-geological and microstructural perspectives. The measurement results illustrate that the microstructures in carbonate rocks are influenced by tectonic-sedimentary patterns and sea level fluctuation. Various rock types are observed: pore type dolomitic gypsum, argillaceous dolomite, and microcrystal dolomite in restricted-evaporative lagoon environments; dissolved pore type and crack-dissolved pore type dolomite in mound-shoal environments; and dissolved pore type gypsum dolomite in platform flat environments. Furthermore, the mineral components as the load-bearing frame and the pore structure jointly control the elastic properties. Samples with the same lithology exhibit similar load-bearing frames, leading to a strong statistical relationship between V_P and V_S. Concerning the pore structure, dissolved pores formed by atmospheric freshwater dissolution during the penecontemporaneous period have high stiffness, minimally affecting the elastic properties of reservoirs. Conversely, the lower stiffness of microcracks resulting from tectonic rupture significantly decreases the P-wave impedance and Poisson's ratio of dry samples, while increasing the Poisson's ratio of water-saturated samples. These findings enable the accurate recognition of the seismic elastic characteristics of high-quality dolomite reservoirs in mound-shoal environments, thus providing a rock physics experimental basis for improving the precision of seismic reservoir prediction in the study area.

1. Introduction

Abundant hydrocarbon resources are distributed in onshore marine carbonate rocks in western China. Large or super large oil and gas fields such as Anyue, Tahe, and Jingbian have been found in marine carbonate strata of the Sichuan Basin, Tarim Basin, and Ordos Basin, respectively (Ma et al., 2017; Zou et al., 2023). Nonetheless, challenges of increasing oil and gas reserves and stabilizing production remain key issues restricting the development of China's petroleum industry, necessitating a new round of hydrocarbon exploration technology revolution. As a crucial stratum in natural gas exploration, the fifth member of the Ordovician Majiagou Formation (M_5) in the Ordos Basin, characterized by a carbonate-gypsum salt rock combination sedimentary system, has garnered significant attention over time. Previously, the primary exploration target was considered to be the weathered crust reservoirs in the upper part of M_5 (Fang et al., 2009; He et al., 2013; Li

* Corresponding author. Key Laboratory of Earth Exploration & Information Technology, Ministry of Education, Chengdu University of Technology, Chengdu, 610059, Sichuan, China.
E-mail address: dengjixin@cdut.cn (J.-X. Deng).

https://doi.org/10.1016/j.petsci.2024.05.024

et al., 2022), while the exploration in M_5 beneath the gypsum salt layer (M_5 subsalt) was relatively limited (Yang et al., 2014). However, recent exploration wells in the Jingbian–Yan'an area of the Ordos Basin have obtained industrial gas flow in dolomite of the M_5 subsalt interval, demonstrating the significant natural gas exploration potential and promising exploration prospects of the marine carbonate reservoirs within the M_5 subsalt (Yu et al., 2018). This highlights the M_5 subsalt as a crucial target for finding new favorable exploration zones and natural gas enrichment areas.

The M_5 subsalt in the Ordos Basin comprises dolomite and gypsum salt, with the gypsum salt layers playing a crucial role in the formation of reservoirs and oil and gas traps. Thus, geologists have progressively investigated the tectonic-sedimentary features, formation conditions, and reservoir formation mechanisms (Ehrenberg, 2006; Chen et al., 2019). Studies have revealed that the carbonate reservoirs of Majiagou Formation underwent a long and intricate geological process, with the tectonic-sedimentary patterns and subsequent diagenetic types determining the development of the carbonate reservoirs. During the Ordovician Majiagou age, the tectonic-sedimentary patterns of the Ordos Basin featured large uplifts and depressions, with high-energy grain shoals in the low uplift zone. In the subsequent diagenetic stage, high-quality dolomite reservoirs formed through constructive diagenesis, such as dolomitization, supergene dissolution, and tectonic activities (Yao et al., 2015, 2016; Fu et al., 2019; Xiong et al., 2019). Clearly, rock properties such as texture, mineral compositions, porosity, pore types, and organic contents are controlled by these complex geological processes, and then affect the elastic properties of carbonate reservoirs (Kenter et al., 1997; Brigaud et al., 2010; Zhao et al., 2013; Abdlmutalib et al., 2019; Teillet et al., 2021; Sharifi, 2022). As an essential tool for predicting hydrocarbon distribution in carbonate reservoirs using seismic attributes, seismic rock physics study can provide critical physical mechanism understanding and constraints for quantitative seismic interpretation of reservoirs. These findings have been successfully applied to seismic exploration. However, systematic rock physics experiments on the carbonates of the M_5 subsalt in the Ordos Basin are deficient, and existing studies focus on the microscopic rock structures without effectively integrating the concept of macro-geological processes controlling rock characteristics. As a result, variations of seismic elastic properties in the region cannot be accurately demonstrated, since rock physics characteristics are summarized through simple experiments without considering the overall control of sedimentary differentiation on rock properties.

On this basis, a set of the M_5 subsalt samples from different sedimentary environments in the Ordos Basin were selected. Then, the ultrasonic velocities (V_P and V_S) of samples were measured under simulated reservoir pressure conditions, and differences of petrological characteristics caused by the tectonic-sedimentary pattern were determined. Next, the controlling effects of geological factors on rock physics properties were discussed. An evolution relationship among sedimentary environment, rock characteristics, and seismic elastic response characteristics is established through velocity response comparisons, providing more accurate geological indications of seismic rock physics properties. This work positively impacts the expansion of seismic rock physics research and improves the accuracy of seismic and logging evaluations.

2. Geological background

The Ordos Basin is a rectangular multi-cycle superposed basin with an area of about 3.7×10^5 km^2 (Fig. 1(a)). During the Ordovician Majiagou age, a large 'L' shaped uplift in the southwestern part of the basin was formed by the subsidence and spreading of the Helan Rift Valley and the shoulder warping, i.e., the Central paleouplift. To the east of the basin, the North Shaanxi depression, with Mizhi-Yan'an as the subsidence center, was formed due to equilibrium adjustment (He et al., 2009; Xi et al., 2023). The Yimeng uplift and Weibei uplift bound the northern and southern parts respectively, establishing a paleotectonic pattern characterized by alternating uplifts and depressions. The study area is situated in the transition zone between the North Shaanxi depression and the Central paleouplift, featuring relatively flat sedimentary paleogeomorphology. Furthermore, the arid climate during the Majiagou period, combined with the barrier effect of paleoland and peripheral uplifts, led to a rhythmic interbedded sedimentary model comprising carbonate (predominantly dolomite) and gypsum salt rock. Vertically, the M_5 is divided into 10 submembers, and M_5 subsalt reservoirs usually refer to the sixth submember of M_5 (M_5^6) to the tenth submember of M_5 (M_5^{10}), as shown in Fig. 1(c). Additionally, controlled by multi-stage secondary sea-level fluctuation and salinity oscillation of sedimentary water, the lithology and sedimentary characteristics of each M_5 subsalt submember exhibit obvious different. During the sedimentary period of M_5^6, M_5^8, and M_5^{10}, sea levels decreased, leading to the predominant development of evaporite rocks, particularly thick gypsum salt rock, interspersed with argillaceous carbonate rock (Xia et al., 2007; Huang et al., 2014). These formations serve as important source rocks and cap rocks for subsalt reservoirs. Conversely, sea levels rose during the sedimentary periods of M_5^7 and M_5^9, resulting in widespread development of carbonate rocks alongside evaporative rock sequences, which also represent target areas for high-quality natural gas reservoirs (Xi et al., 2017).

3. Sample description and rock physics measurements

Samples used in all experiments were drilled from target exploration strata in the central Ordos Basin (Fig. 1(b)). To ensure the experimental results are representative, a sufficient number of samples were taken from well of T58, Jt1, J5, and Sh473 (detailed coring well distribution is shown in Section 4.1), covering the main rock types developed in each sedimentary environment of the study area. A total of 101 one-inch (25.4 mm) plugs were drilled. All plugs were cut to an average length of 50 mm, and the end faces were ground to a tilt of less than 0.01 mm. Additionally, parts of each plug were used to make thin sections for mineral composition analysis, ensuring quality and thickness according to experimental standards. The porosity was measured with a helium porosimeter, with a measurement range of 0.01%–40%. Here, a plot of porosity for the M_5 subsalt carbonate as a function of confining pressure is provided (Fig. 2). The porosity decreases slightly with the increase of confining pressure (a decrease of about 5%), likely due to the rigidity of the carbonate rock skeleton. Therefore, when measuring the porosity of all samples, the influence of confining pressure on the porosity was ignored in order to simplify the experimental procedure, and the confining pressure was set to 40 MPa. Furthermore, the mineralogical characteristics (mineral composition) were quantitatively identified using X-ray diffraction techniques. Polarized optical microscopy was used to observe polished thin sections of typical samples to analyze rock structure characteristics. Finally, the V_P and V_S of samples were measured by ultrasonic pulse transmission technique. The peak frequencies of the compressional wave (P-wave) transducer are 800 kHz and 350 kHz for the shear wave (S-wave) transducer. Velocities were calculated by using the ratio of sample length and travel time. For measuring the acoustic velocities of dry and saturated samples in the laboratory, all samples were placed in an oven (70 °C) for more than 72 h and then exposed to humid air (50%–60% humidity) for about 48 h, reaching dry condition (about 2%–3% moisture content) required for the experiment. Subsequently, samples were placed in a

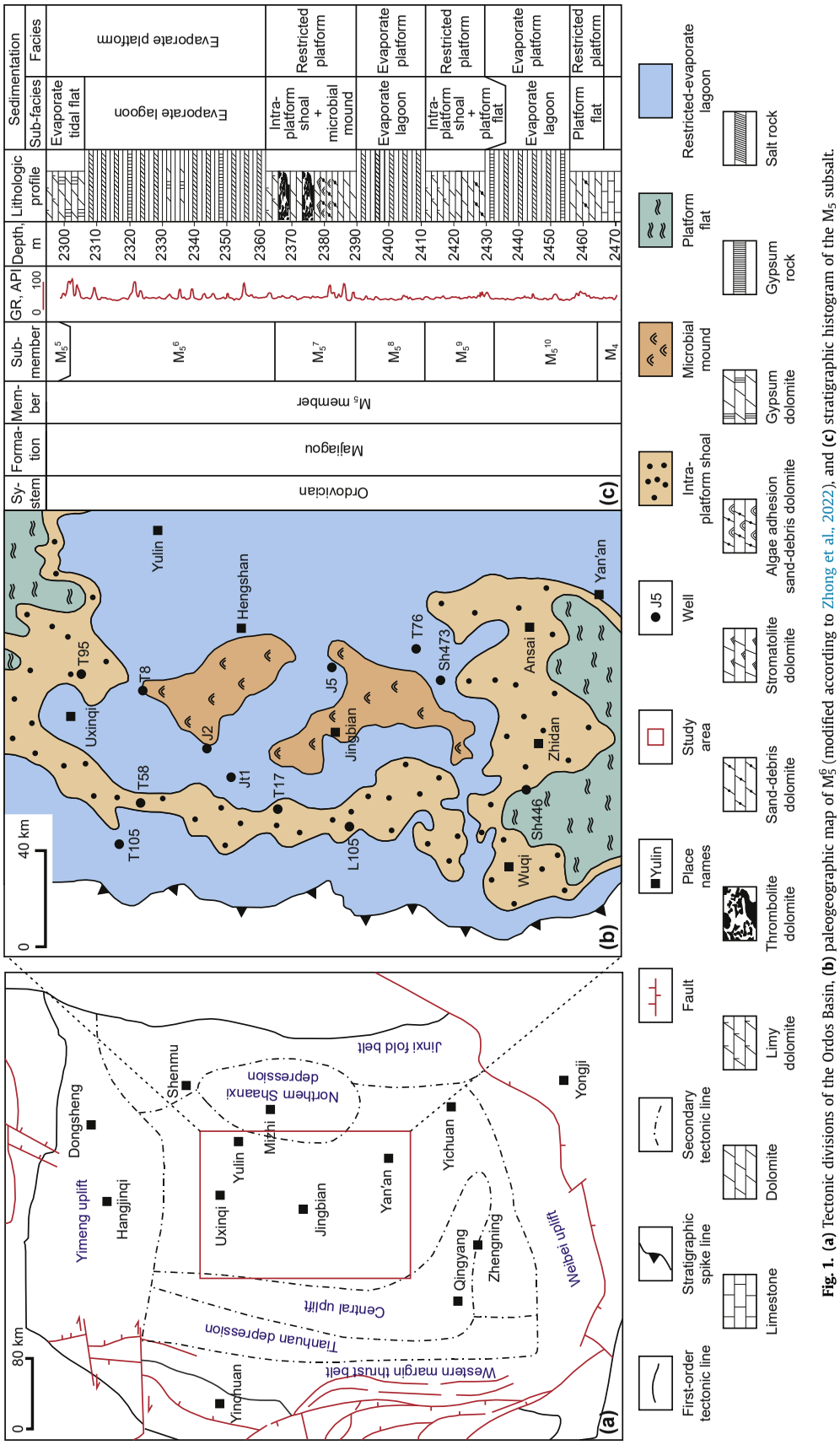

Fig. 1. **(a)** Tectonic divisions of the Ordos Basin, **(b)** paleogeographic map of M_5^6 (modified according to Zhong et al., 2022), and **(c)** stratigraphic histogram of the M_5 subsalt.

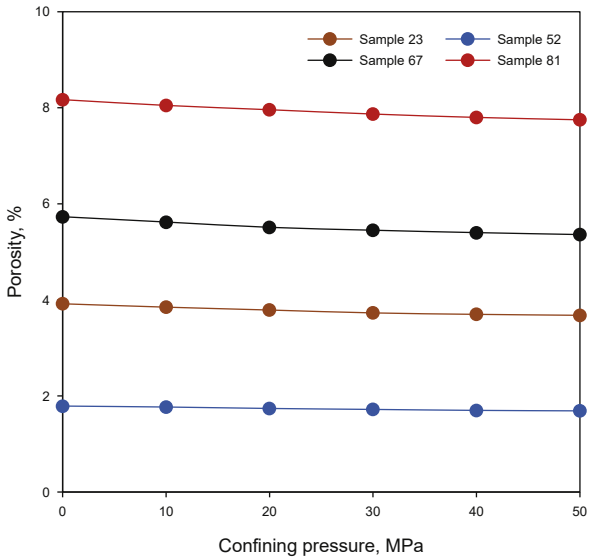

Fig. 2. Porosity of the plugs for the M_5 subsalt carbonate rock as a function of confining pressure.

container with 3% NaCl solution (to avoid potential chemical reactions) and stored under vacuum conditions for at least 24 h to ensure saturation. During the measurement, the confining pressure was gradually increased (0, 2, 5, 10, 20, 30, 40, and 50 MPa) to the pressure value corresponding to the average depth of the M_5 subsalt. Each sample was measured after reaching the preset confining pressure value for 30 min to ensure uniform pressure distribution. According to the error analysis method proposed by Yin (1992) and Hornby (1998) for ultrasonic pulse transmission experiments, the maximum absolute error in the measurement is

$$\Delta V = \frac{\Delta L}{t_M - t_T} + 2L\frac{\Delta t}{(t_M - t_T)^2} \quad (1)$$

where L is sample length, t_M is the measured travel time through the sample, t_T is a reference travel time from the head-to-head measurement, Δt is the error in the travel time picks, and ΔL is the magnitude of the error in the sample length measurement. Fig. 3 shows representative waveforms for the compressional wave (P-wave) and shear wave (S-wave), with first zero-crossing arrival times chosen. To estimate errors, a typical sample length of 50 mm was considered, with a precision of sample length measurement of 0.2% or 0.1 mm. For P-wave propagation, a typical value for $(t_M - t_T)$ is 8 μs, with a precision of travel time picking equal to the sampling rate of 0.02 μs. Consequently, the absolute error of the velocity measurement was estimated 47 m/s, and the relative error in the velocity estimation of approximately 0.8 percent for a P-wave propagating at a velocity of 6200 m/s. Similarly, the relative error in V_S estimation is approximately 1.2%. Based on the above experiments, we analyzed the variation of rock physics properties of carbonate reservoirs in the M_5 subsalt within the geological framework.

4. Results and analysis

4.1. Petrological characteristics

The restricted-evaporative epicontinental sea carbonate platform developed widely during the M_5 sedimentary period under the backdrop of large-scale regression (Fu et al., 2019). Based on differences in mineral composition, lithology, and texture of carbonate samples, and referencing the lithofacies paleogeography of the Majiagou age in the Ordos Basin (Feng and Bao, 1999) and the sedimentary model of each submember in M_5 (Xi et al., 2017), the sedimentary environments of the M_5 subsalt carbonate rocks in the study area are divided into four types: restricted-evaporative lagoon, intra-platform shoal, microbial mound, and platform flat (Fig. 4).

1 Restricted-evaporative lagoon: This type is located in the underwater low-lying area within the platform and is widely distributed in the study area. It is mainly found in M_5^6, M_5^8, and M_5^{10} (with a small amount of development in M_5^7 and M_5^9), and develops dolomitic gypsum and microcrystal dolomite (Fig. 5(a)–(d)). The anhydrite content of the dolomite gypsum is about 50%–80%, and light gray-gray white rhythm stripes are visible in most samples. The anhydrites (with a size of about 0.02 mm × 0.15 mm) are mostly distributed in a plate-like or needle-like radial patterns under the microscope. The microcrystal dolomite is mostly beneath the dolomitic gypsum, which is light gray-dark gray dense massive in macroscopic view. The dolomite content is high, and the anhydrite content is very low (less than 5%). Moreover, the grain diameter of dolomite is usually less than 5 μm, and grains are densely embedded in contact. In addition, the rocks developed in this sedimentary type often contain a certain amount of clay, and dark horizontal argillaceous stripes can be seen locally under the microscope.
2 Intra-platform shoal: This type is located in the underwater positive landform uplift areas within the platform and frequently occurs in the target zone. It is mainly found in M_5^7 and M_5^9 and develops sparry sand-debris dolomite and crystalline dolomite (Fig. 5(e), (f)). The sand debris content is 60%–75%, with better sorting and rounding, and most particles are subrounded to rounded. The sand debris is mostly in point-line

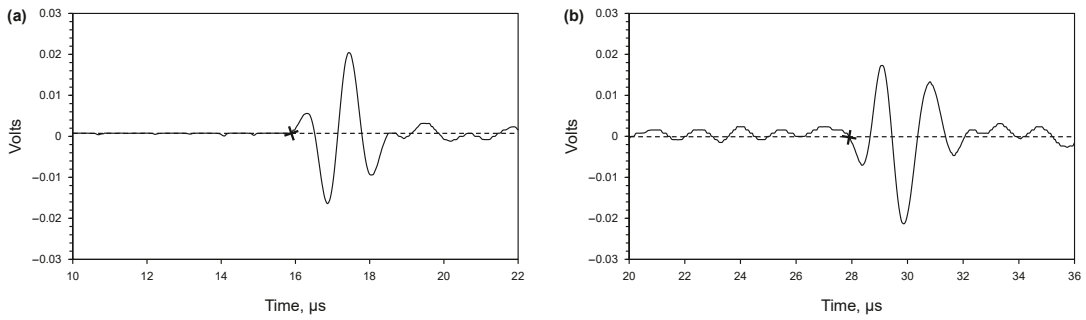

Fig. 3. Representative ultrasonic waveforms for **(a)** the compressional wave and **(b)** the shear wave for a sample of the M_5 subsalt. First zero-crossing arrival time picks are indicated on the waveforms (crosses).

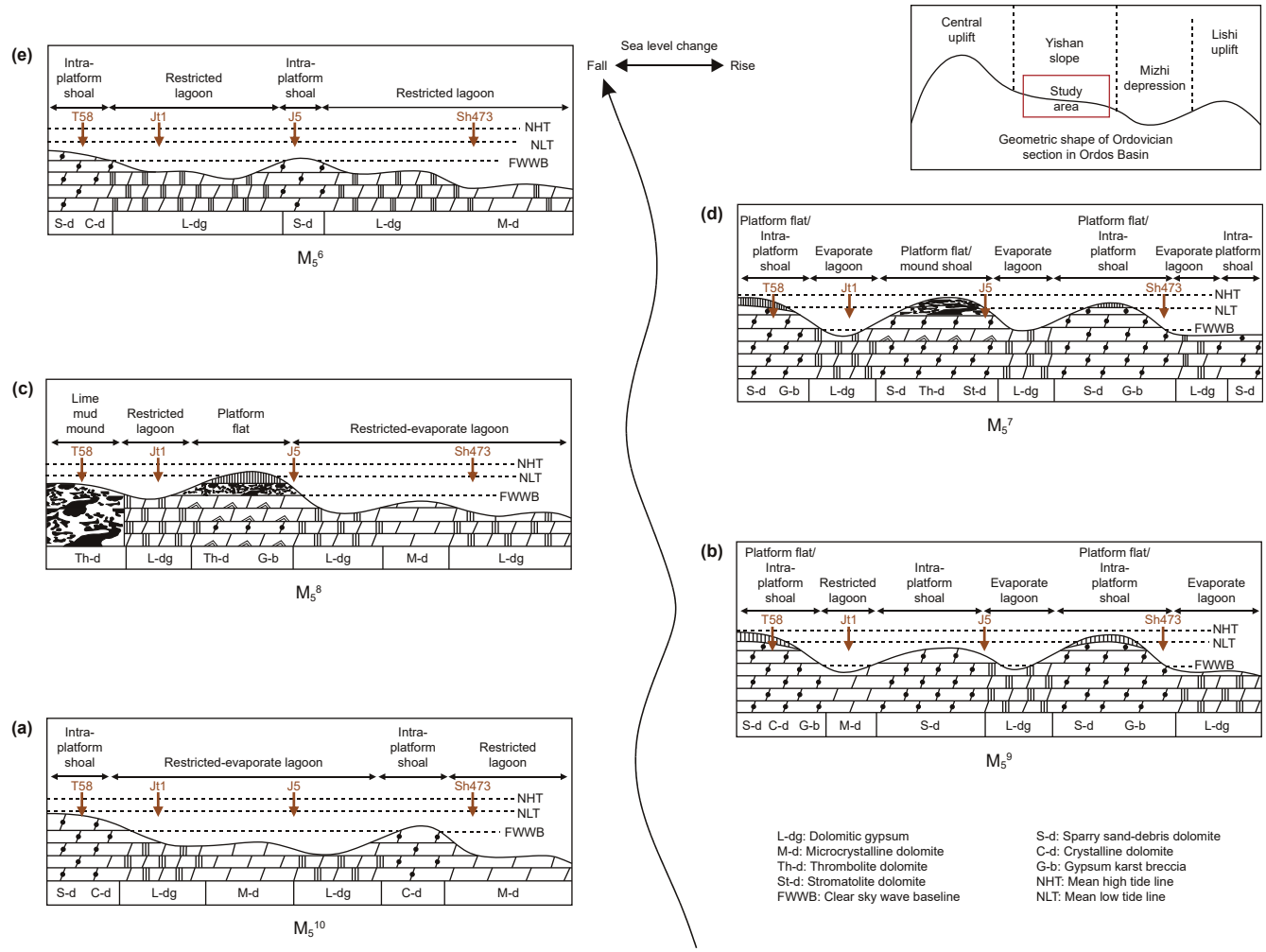

Fig. 4. Sedimentary environment evolution model and sea level change of the M_5 subsalt in the central Ordos Basin (modified according to Xi et al. (2017). **(a)** Sedimentary environment of M_5^{10}; **(b)** sedimentary environment of M_5^9; **(c)** sedimentary environment of M_5^8; **(d)** sedimentary environment of M_5^7; **(e)** sedimentary environment of M_5^{10}.

contact, filled with bright crystalline dolomite or asphalt. The dolomite content of crystalline dolomite is usually more than 90%, and powder crystal or fine crystal dolomite is idiomorphic-hypidiomorphic and closely inlaid.

3 Microbial mound: This type is mostly on the grain shoal or associated with the grain shoal, and a large number of microbials were developed. Drilling results show that this type is widely developed in M_5^7 and M_5^9. It mainly develops clotted dolomite, composed of reticular or clustered dark condensates and sparry dolomite cements (Fig. 5(g)). More precisely, the compositions of clots are microcrystal dolomite, and a small amount of anhydrite is distributed in the clot. The cementing materials between clots are mainly the bright crystal dolomite. Owing to the distribution and hydrodynamic conditions of microbial mounds and intra-platform shoals are similar, we collectively refer to these two types as the mound-shoal environment in the subsequent rock physics analysis.

4 Platform flat: This type is mostly above the grain shoal or microbial mound in the vertical direction and is frequently developed in the study area. Stromatolite dolomite and gypsum karst breccia are the most common rock types in the platform flat (Fig. 5(h) and (i)). Stromatolite dolomite is characterized by the repeated alternation of dark algae-rich layers and bright algae-poor layers, mostly horizontal and microwave-like in morphology. The dark layers are composed of algae-rich micrite dolomite, with high organic matter content. The bright layers are composed of mud powder crystal dolomite and anhydrite crystal, with a thickness of 1–5 mm. The main component of gypsum karst breccia is anhydrite, and milky white breccias with various shapes (square, triangle, or irregular diamond) can be observed. Most of the breccias are filled with gray-brown calcite or black clay related to leaching and infiltration.

4.2. Pore spaces and physical properties

The pore types of the M_5 subsalt carbonate samples in the study area are extremely complex. Main types include inter-crystalline pores, inter-crystalline dissolved pores, inter-granular dissolved pore, intra-granular dissolved pore, gypsum mould pore, filling residual vug, and micro crack, as summarized in Fig. 6.

1 The inter-crystalline pore and inter-crystalline dissolved pore: The inter-crystalline pores are mainly developed in the crystalline dolomite with higher euhedral degree, and pores are formed by point contact or lap contact between grains. Most of them are irregularly serrated and have good connectivity. The pore size ranges from 0.05 mm to 0.5 mm. Moreover, affected by

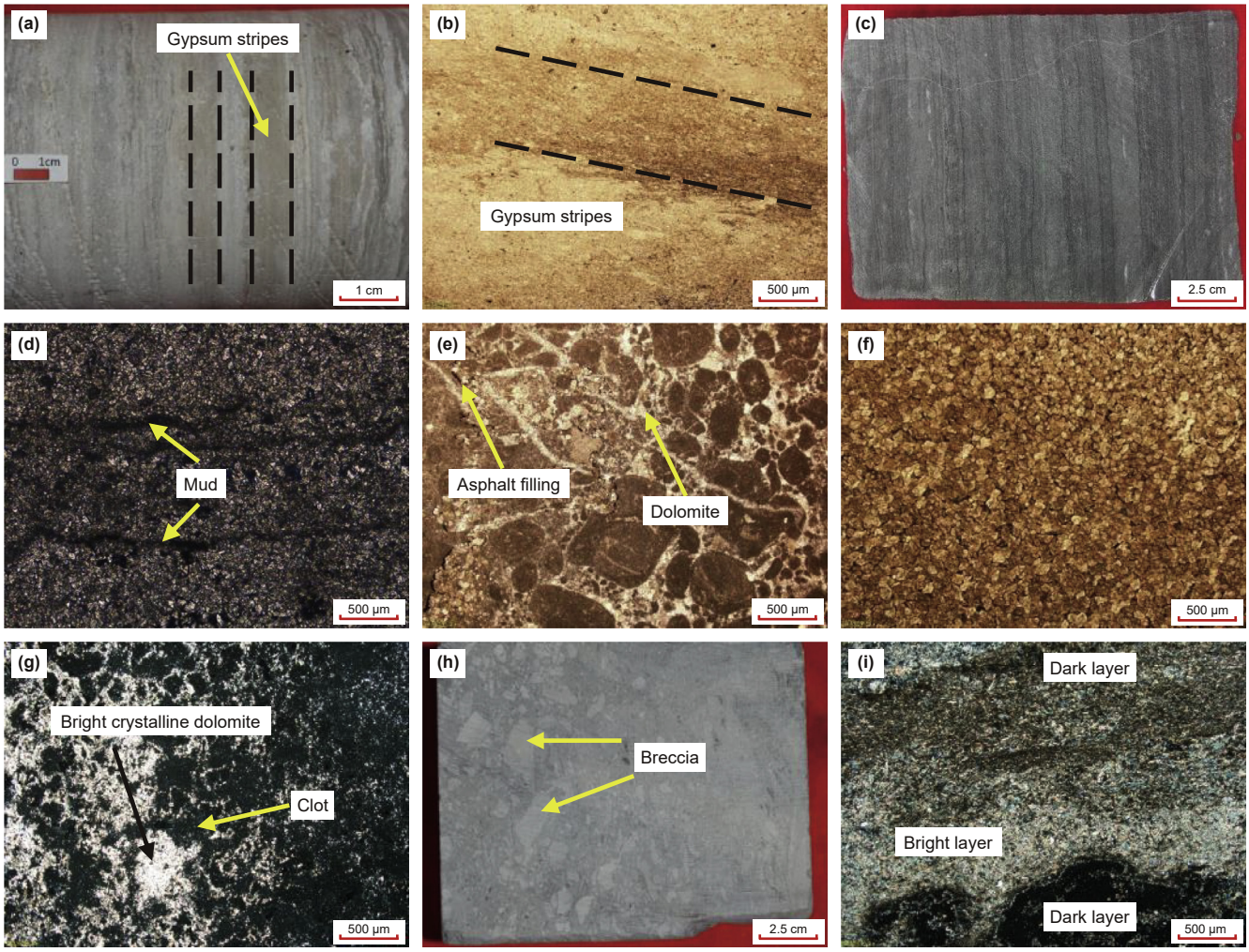

Fig. 5. Petrological characteristics of the M_5 subsalt samples. **(a)** Dolomitic gypsum, gray-white gypsum and light gray gypsum dolomite are frequently interbedded, well Sh473; **(b)** dolomitic gypsum, gypsum and gypsum dolomite are interbedded, casting thin section, plane-polarized light (PPL), well Sh473; **(c)** microcrystal dolomite, dark horizontal muddy stripes are visible, well Jt1; **(d)** argillaceous dolomite, muddy stripes are visible, ordinary thin section, PPL, well Jt1; **(e)** sand-debris dolomite, sand debris is mostly point-line contact, intergranular is filled with bright crystalline dolomite or asphalt, casting thin section, PPL, well J5; **(f)** crystalline dolomite, idiomorphic-hypidiomorphic, grains are closely inlaid, casting thin section, PPL, well Jt1; **(g)** clotted dolomite, clots are mainly characterized by dark cluster shape, and the cement crystals between the clots are relatively coarser, casting thin section, PPL, well T58; **(h)** gypsum karst breccia, milky white gypsum breccia is mostly triangular or irregular diamond, well T58; **(i)** stromatolite dolomite, dark layer is composed of bacteria-rich algae micritic dolomite with high organic matter content, while bright layer is composed of micritic dolomite and anhydrite crystals, which are undulating distributed, casting thin section, PPL, well J5.

the later burial dissolution, the areas with better physical properties can further form inter-crystalline dissolved pores, and the pore edge is harbor-shaped. They are an important nature gas reservoir space in the M_5 subsalt, which are often developed in the powder-fine crystal dolomite (Fig. 6(a)).

2 The inter-granular and intra-granular dissolved pore: These types are the product of the penecontemporaneous atmospheric freshwater dissolution, mostly irregular and often developed in the sand-debris dolomite. Affected by the late diagenesis, some pores are filled or semi-filled with anhydrite, authigenic quartz, or fine-medium crystal dolomite cements (Fig. 6(b)).

3 Gypsum mould pore: These pores can be divided into two types. The first type was formed by the penecontemporaneous dissolution. The pores still retain the original anhydrite morphology because the anhydrite columnar crystals associated with the crystalline dolomite were only dissolved early (Fig. 6(c)). The second type was formed by the metasomatism of calcite in the burial period, and pyrite was developed around pores.

4 Filling residual vug: This type results from strong penecontemporaneous exposure and dissolution of sediments in high-energy mound-shoal environments, and bedding-distributed vugs with a diameter of 2–10 mm can be seen on cores (Fig. 6(d)). Most of vugs are disorderly filled by various types of collapsed breccia.

5 Micro crack: The Ordos Basin experienced multi-stage tectonic activities after the Majiagou age. Although tectonic ruptures should form a fracture system to improve reservoir seepage capacity, the frequency and scale of tectonic fractures in the study area are small, and most are filled with deposits (Fig. 6(e)). This phenomenon may relate to the suspension uplift and decompression effect caused by the symbiotic combination of gypsum-salt and carbonate (Xia et al., 2009). The fracture types here are mainly small irregular dissolved cracks (core-scale microcracks), which have little reservoir significance and only slightly increase local permeability (Fig. 6(f)).

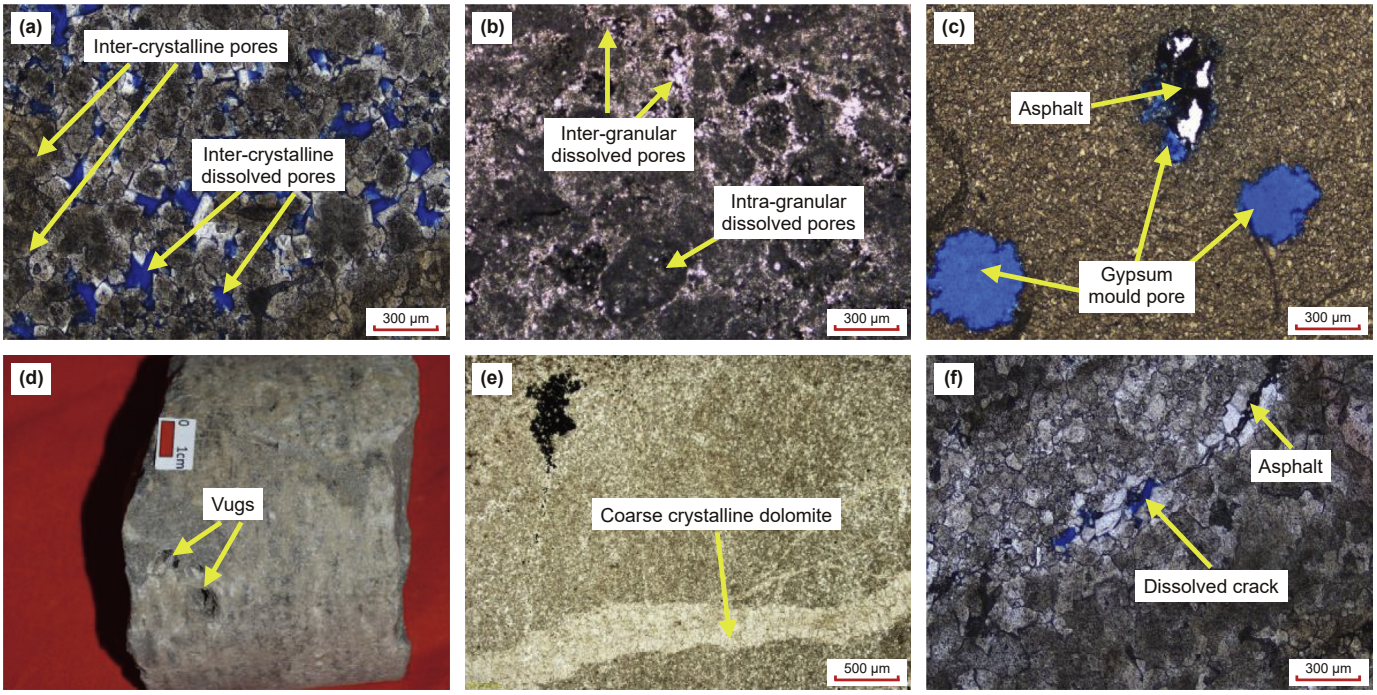

Fig. 6. Pore structure characteristics of the M_5 subsalt samples. **(a)** Inter-crystalline pore and inter-crystalline dissolved pore; **(b)** inter-granular and intra-granular dissolved pore, and pores are filled with dolomite; **(c)** gypsum mould pore, isolated; **(d)** filling residual vug, bedding-distributed; **(e)** cracks are filled with coarse grained dolomite; **(f)** dissolved crack, part of the space is filled with asphalt.

The pore type trends are also considerably correlated with the sedimentary environment. Four pore type combination are classified in accordance with the differences in the development characteristics of rock reservoir space, namely, crack-dissolved pore type, dissolved pore type, crack-pore type, and pore type. The crack-dissolved pore type and dissolved pore type are mainly developed in the samples come from the mound-shoal and the platform environment, and the dissolved pores are connected by straight or curved microcracks of different scales. While the crack-pore type and pore type are mainly developed in samples come from the restricted-evaporative lagoon environment, and the connectivity between pores is relatively poor.

The porosity measurement result shows that the porosity of the M_5 subsalt samples is 0.7%–8.9%, but a simple positive or negative correlation between the porosity and the mineral components content is not acquired. However, when displaying the sedimentary environment and lithological variations, we observe a clear clustering of the data (Fig. 7). This correlation reflects the control of the tectonic-sedimentary pattern on the primary pores and then the positive effect of dolomitization on the pore space preservation. After the accumulation of grain shoal, original pores were formed between the grains, and the porosity was generally as high as 40%–60% (Zhou et al., 2015). Subsequently, the porosity decreased rapidly by cementation, but it still provided an essential basis for the formation of high-quality reservoirs. Compared with calcite, dolomite with higher hardness can effectively resist the mechanical compaction caused by the overlying sediments. Thus, the sediments were dolomitized and the pores were largely protected under the penecontemporaneous Sabkha dolomitization and seepage-reflux dolomitization. These geological factors eventually result in relatively higher porosity of dolomite samples in high-energy environments. On the contrary, some samples developed in the lagoon environment show a data feature of low porosity and high dolomite content, which reflects that the low water energy resulted in low deposition rate, small granular size, and relatively low original porosity. Although early dolomitization was also widespread in these sediments, the anti-compaction ability was limited and the pore was obviously destroyed. Moreover, original sediments were not exposed to the atmospheric freshwater, and dissolution transformation was very weak. Different from dolomite, a weaker correlation between the porosity and dolomite/anhydrite content of gypsum rock samples can be observed (Fig. 7(b)). However, the porosity of samples developed in the platform flat is significantly greater than that in the lagoon, which also reflects the crucial role of atmospheric freshwater dissolution transformation on reservoir quality under the control of tectonic-sedimentary pattern. As mentioned above, the gypsum rocks deposited in the low-energy lagoon (lower part of the landform) lack the stage of exposure to freshwater, the pores are not developed, and the porosity is generally low. While the gypsum rocks developed in the platform flat were located in the high part of the landform during the sedimentary and early diagenetic stages. The gypsum substances (solubility is much greater than dolomite) in the sediments were dissolved in the short-term exposure process to form gypsum mould pores, owing to the multi-period transgression-regression cycles (sub-level) in the penecontemporaneous stage (Xi et al., 2017). Although partially filled in the late stage, those gypsum mould pores are still the unique reservoir space of the M_5 subsalt reservoirs.

4.3. Density characteristics

The bulk density of the M_5 subsalt samples displays a wide range of values from 2.58 g/cm^3 to 2.97 g/cm^3, and density and anhydrite content present a strong correlation. The fundamental reason for a positive correlation between density and anhydrite is that the main minerals (anhydrite: 2.98 g/cm^3, dolomite: 2.87 g/cm^3, clay: 2.60 g/cm^3; according to Mavko et al. (2009) of the M_5 subsalt samples, especially anhydrite crystals. A negative correlation between density and porosity is also clearly observed, which is consistent with

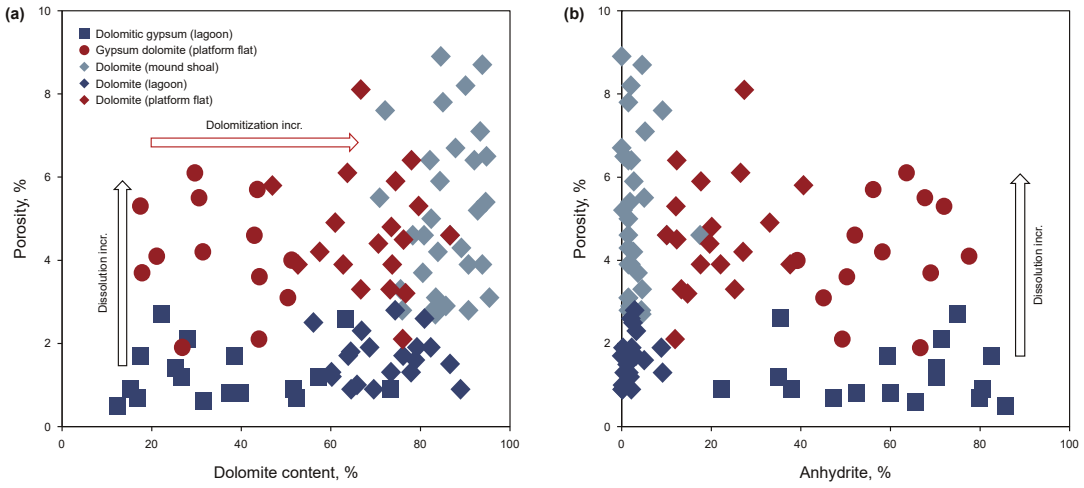

Fig. 7. Relationship between porosity and the main mineral components **(a)** dolomite content; **(b)** anhydrite content for the M_5 subsalt samples.

the existing understanding that density is a decreasing function of porosity. Fig. 8 also shows the evolution of density is marked by several trends along with the depositional environment. According to the described results in Sections 4.1 and 4.2, the samples developed in the lagoon are mainly affected by the mineral composition because the penecontemporaneous dissolution is extremely weak (porosity is mostly below 2%). In view of this, we can observe that the porosity has almost no substantial effect on the density value. The data of these samples are distributed in two different regions with the rapid change of anhydrite content. Conversely, the samples come from the platform flat environment and mound-shoal environment were affected by strong dissolution during the penecontemporaneous period, and secondary pores were developed, as a result, the density decreases with the increase of porosity. Moreover, the samples developed in the platform flat tend to have the higher density for a given porosity, since gypsum materials were mostly deposited in the platform environment with high-salinity seawater.

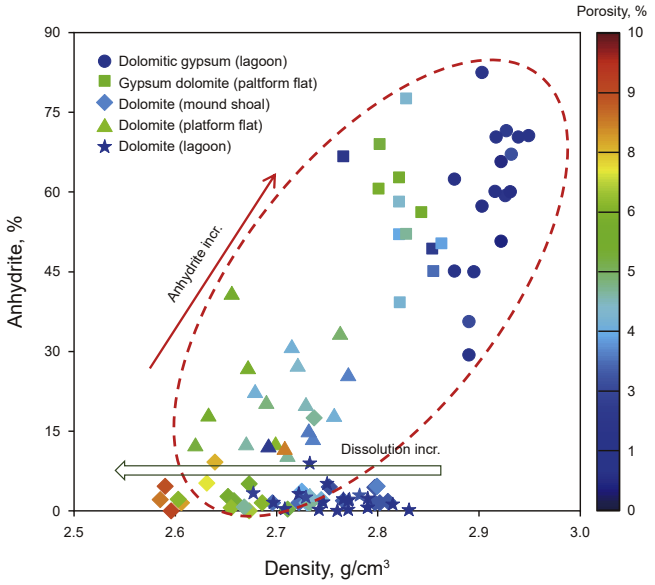

Fig. 8. Density response for the M_5 subsalt samples with change of anhydrite and porosity.

4.4. Seismic elastic characteristics

According to the mineralogy and pore characteristics of samples developed in different sedimentary environments, the samples collected in this experimental study are divided into six types: pore type dolomitic gypsum rock, dissolved pore type gypsum dolomite, pore type argillaceous dolomite, pore type dolomite, dissolved pore type dolomite and crack-dissolved pore type dolomite. In this section, the variation laws and controlling factors of elastic property response of the M_5 subsalt carbonate reservoir are analyzed by applying these classifications.

4.4.1. Velocities versus confining pressure

The response of measured P- and S-wave velocities to confining pressure is controlled by the combination type of pore structure. Two variation pathways of the P- and S-wave velocities of dry carbonate rock samples increase with increasing pressure are observed in Fig. 9: (1) the P- and S-wave velocities increase significantly in the low-pressure interval and slowly in the high-pressure interval, (2) the P- and S-wave velocities increase gradually at a stable rate. A suitable explanation is the high-pressure sensitivity of microcracks or intergranular cracks. The crack-dissolved pore type samples mostly correspond to pathway (1). During the progressive loading process, the flat cracks with smaller stiffness tend to be closed, resulting in a significant increase in velocity. Then the microcracks are completely closed in the high-pressure range (the equiaxed or ellipsoidal pores are less sensitive to pressure), and the velocities increase steadily. The pore elastic properties of the pore type sample or the dissolved pore type sample are relatively uniform, so the velocity response mode corresponds to pathway (2), which is similar to the change after the critical pressure (approximately 30 MPa) of pathway (1). In the water-saturated samples, the compressibility of microcracks can be decreased by filling fluid, resulting in a weakening of the velocity pressure effect. Thus, a trend consistent with that of the dry sample can be observed in Fig. 9(c), (b), but the rangeability is relatively narrow. In contrast, the obvious change in the velocity pathway of the pore type argillaceous dolomite is not observed, except for the overall decrease in the velocity value. This indicates that the mineral composition has little effect on pressure.

4.4.2. V_P and V_S relationship

Fig. 10 shows the V_P and V_S relationship of the M_5 subsalt samples under the reservoir pressure condition. For comparative

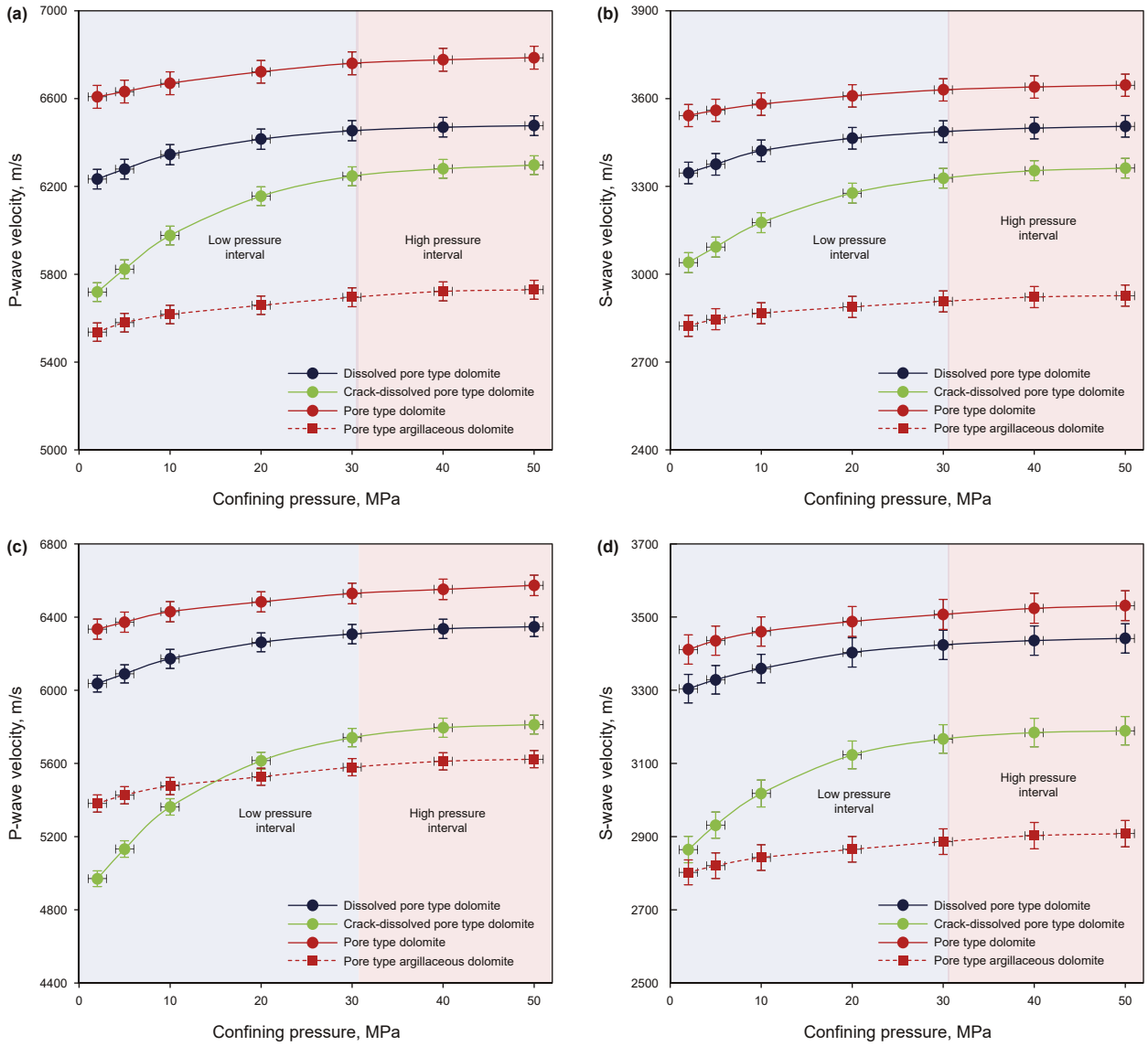

Fig. 9. Response of P- and S-wave velocities when the confining pressure is increasing under different fluids saturation. **(a)**, **(b)** showed V_P and V_S in the dry condition; **(c)**, **(d)** showed V_P and V_S in the water-saturated condition.

purposes, the ultrasonic velocities (V_P & V_S) data of M_5^5 limestone and V_P and V_S relationships of the saturated limestone and dolomite (hereafter referred to as "limestone line" and "dolomite line"; Pickett, 1963) are drawn in Fig. 10. Obviously, when samples are discriminated by their lithology on the crossplot of V_P and V_S, the data distribution displays a good correlation. This clear clustering appears can be explained by load-bearing frame. The elastic properties of same lithology samples are highly similar, because their similar load-bearing frame. On the contrary, the obvious change in load-bearing frame type of different lithology samples contributes to the downward or upward migration of V_P and V_S relationship (Fig. 10(a)). Moreover, when displaying pore structure, crack-dissolved pore type dolomite samples deviate from the dolomite line. For the pore type, dissolved pore and crack-dissolved pore type dolomite samples, the load-bearing frame are basically dolomite grains. At this point, velocities of rock medium are less affected by other minerals, and the V_P and V_S relationship is close to the dolomite line. Under the dry condition (gas-saturated), the micro-cracks with minimal stiffness have a dramatic decrease in V_P, resulting in a downward deviation of the data from the dolomite line. Instead, the V_P and V_S relationship of pore type and dissolved pore type dolomite samples has not changed significantly because the effects of pores or dissolved pores on the V_P and V_S are similar. Under the water-saturated condition, the stiffness of soft pores increases significantly, and the dispersion effect caused by squirt flow is superimposed. And that is why the increase of V_P is significantly greater, and the distribution of crack-dissolved pore type samples to deviate upward from the dolomite line.

4.4.3. The change in P-wave impedance and Poisson's ratio

The change in P-wave impedance and Poisson's ratio of the M_5 subsalt samples are also controlled by mineral composition, pore structure and pore fluid. Fig. 11(a) shows that the P-wave impedance of argillaceous dolomite, gypsum dolomite, limestone and dolomite with the same pore structure type increases gradually, and the Poisson's ratio of gypsum dolomite, dolomite, limestone and argillaceous dolomite increases gradually, which is consistent with the change trend of mineral elastic properties. In detail, the

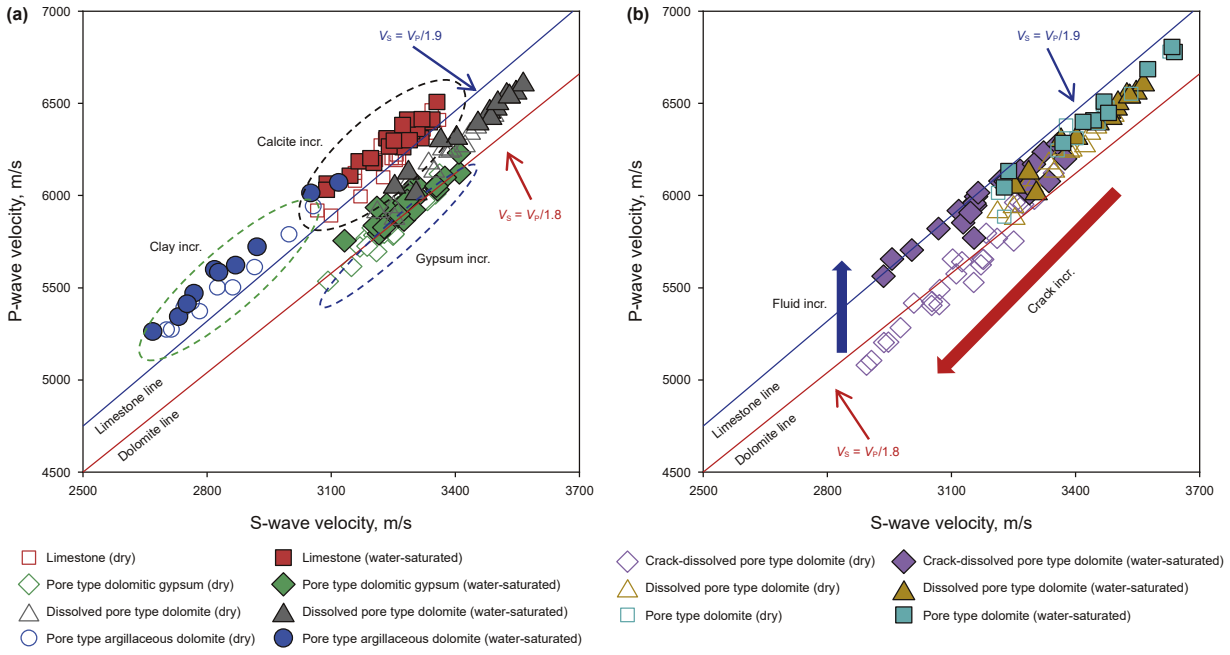

Fig. 10. V_P and V_S relationship of the M_5 subsalt samples. **(a)** showed V_P and V_S relationship of different lithology samples; **(b)** showed V_P and V_S relationship of different pore structure samples.

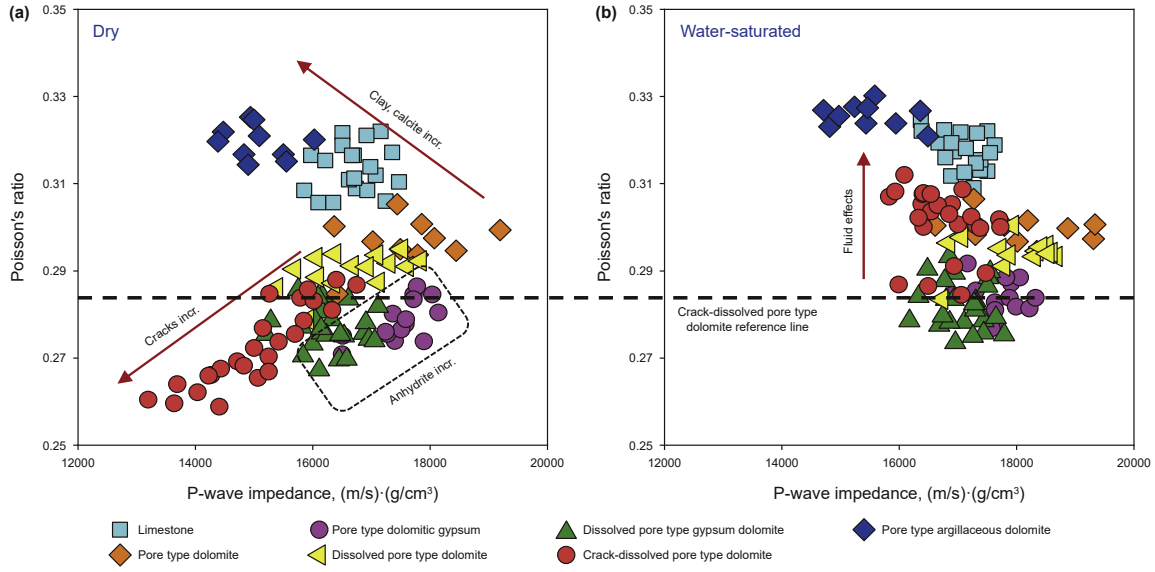

Fig. 11. Change in P-wave impedance and Poisson's ratio of the M_5 subsalt samples under different fluids saturation. **(a)** showed P-wave impedance and Poisson's in the dry condition; **(b)** showed P-wave impedance and Poisson's in the water-saturated condition.

major minerals as load-bearing frame exhibit specific regularity in their elastic properties. According to the rock physics handbook (compiled by Mavko et al., 2009), the P-wave velocity: clay (3400 m/s) < anhydrite (6010 m/s) < calcite (6640 m/s) < dolomite (7340 m/s), velocity ratios (V_P divided by V_S): anhydrite (1.80) < dolomite (1.85) < calcite (1.93) < clay (2.09). Generally, multiple load-bearing frame types may be developed in one sample, and hence the contribution of each type is difficult to be quantitatively analyzed. However, a positive correlation exists between the development ratio of load-bearing frame and the mineral content. It is appropriate to approximate the effect of the type of load-bearing frame on the elastic properties to that of the mineral composition. One interesting observation is that the P-wave impedance and Poisson's ratio of partial dry crack-dissolved pore type samples are even lower than those of dolomitic gypsum rocks, indicating that the effects of microcracks on elastic properties are possibly principal. Furthermore, as mentioned in Section 4.4.1, soft pores have different effects on V_P and V_S with the change of fluid properties. Affected by increase of microcracks, the P-wave impedance and Poisson's ratio of dry samples gradually decrease, and the P-wave impedance of water-saturated samples decreases while Poisson's ratio increases (Fig. 11(b)). Overall, from the perspective of reservoir seismic prediction, the change in P-wave impedance and Poisson's ratio can be utilized to identify gas-

bearing crack-dissolved pore type dolomite, dissolved pore type dolomite and dissolved pore type gypsum dolomite. The commonality of these types of reservoirs is that they were transformed by atmospheric freshwater dissolution during the penecontemporaneous period.

4.4.4. The change in porosity and ultrasonic velocity

Fig. 12 displays that the ultrasonic velocities (V_P & V_S) of samples decrease with the increase of porosity as a whole, but also the trend of each type is obviously different. Owing to the porosity of pore type samples is extremely low, and the pore types are relatively single, the elastic properties of minerals are the primary factor causing a significant change in the ultrasonic velocities. Alternatively, the ultrasonic velocities of dolomite samples with relatively single composition also show great variation under the same porosity. The maximum differences between crack-dissolved pore type and dissolved pore type dolomite (the lowest red circle to the highest yellow triangle in Fig. 12) are close to 1300 m/s (V_P) and 550 m/s (V_S), respectively. Here the ultrasonic velocities change of samples can be considered to be mainly determined by pore structure, rather than porosity. In order to quantitatively analyze the effects of mineral composition and pore structure on P- and S-wave velocities, the differential equivalent medium (DEM) model (Berryman, 1992) is used to calculate the porosity-velocity change relationship under different schemes of composite minerals and pore aspect ratios as shown in Fig. 12. According to this method, the equivalent bulk modulus K^* and shear modulus μ^* of rock can be calculated by the following formula:

$$\begin{cases} (1-\varphi)\dfrac{\mathrm{d}}{\mathrm{d}\varphi}[K^*(\varphi)] = \dfrac{1}{3}(K_i - K^*)T_1(\varphi) \\ (1-\varphi)\dfrac{\mathrm{d}}{\mathrm{d}\varphi}[\mu^*(\varphi)] = \dfrac{1}{5}(\mu_i - \mu^*)T_2(\varphi) \end{cases} \tag{2}$$

The initial conditions are $K^*(0) = K_0$ and $\mu^*(0) = \mu_0$, which represent the bulk modulus and shear modulus of the mineral matrix. Here, K_0 and μ_0 are obtained by mixing minerals with different volume fractions using the Reuss-Voigt-Hill average model (Mavko et al., 2009). φ is the total porosity of samples, and α is the pore aspect ratio. K_i and μ_i are the bulk and shear modulus of the inclusions (dry cracks and pores), respectively, which can be simulated by setting them to zero. T_1 and T_2 are the geometric factors of inclusions, which are related to the aspect ratio (α) of inclusions. The setting schemes of composite minerals and pore aspect ratios for model lines in Fig. 12 are given in the following.

Black dotted line: 90% dolomite and 10% calcite with $\alpha = 0.01$, 0.05, 0.1, 0.2, and 0.8, respectively.
Red solid line: 15% clay and 85% dolomite with $\alpha = 0.2$ (intergranular pores).
Blue solid line: 75% anhydrite and 25% dolomite with $\alpha = 0.8$ (dissolved pores).

After the elastic modulus is obtained, the V_P and V_S of dry condition can be further calculated:

$$\begin{cases} V_P = \sqrt{\dfrac{K^* + (4/3)\mu}{\rho}} \\ V_S = \sqrt{\dfrac{\mu}{\rho}} \end{cases} \tag{3}$$

where, ρ is the density of rock. The pore type and dissolved pore type dolomite samples are mostly distributed above the black dotted line of $\alpha = 0.1$. While the crack-pore type dolomite samples are mainly distributed below the black dotted line of $\alpha = 0.1$, and gradually move closer to the black dotted line of $\alpha = 0.01$ with the increase of microcracks. Affected by the elastic properties of minerals, pore-type dolomite and dissolved pore-type dolomite samples are mainly concentrated near the blue solid line of $\alpha = 0.8$, and pore-type argillaceous dolomite is mainly concentrated near the red solid line with $\alpha = 0.2$. According to the matching relationship between the experimental data and model lines, the lithology and pore characteristics of rocks can be determined, and the analysis results are supported by rock mineralogy and pore structure characteristics in Sections 4.1 and 4.2. In summary, the mineral composition of rock load-bearing frame and pore structure control the seismic elastic characteristics of the M_5 subsalt samples, with porosity playing a secondary role. In the seismic prediction, the effects of lithology and pore structure on velocities should be distinguished, so as to improve the accuracy and precision of gas-bearing carbonate reservoir prediction.

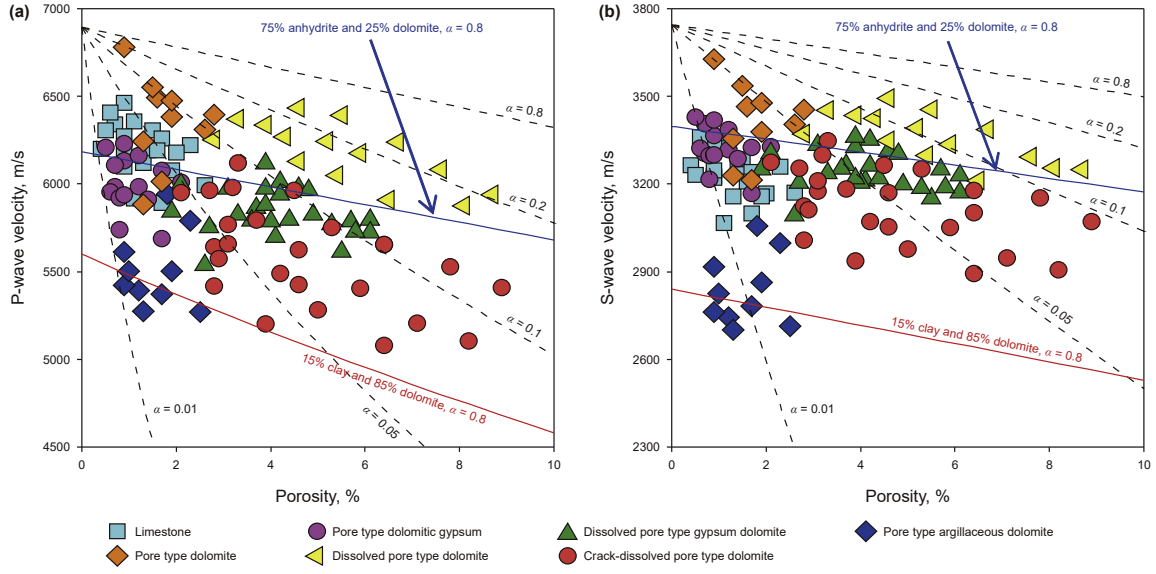

Fig. 12. Response of V_P and V_S with porosity change for the M_5 subsalt samples. **(a)** showed V_P; **(b)** showed V_S.

5. Discussion

5.1. Response of rock microscopic characteristics for geological factor

Following a thorough analysis of all properties available, the microscopic characteristics closely related to the sedimentary-diagenetic environment control macroscopic rock physics properties of rock medium. Therefore, for purpose of further establishing the relationship between geological factors and rock physics properties, we analyzed the rock load-bearing frame characteristics of samples under different sedimentary environment from the geological process. This both gives geological significance to the rock physics properties and reflects changes in reservoir characteristics in the region. Typically, the sedimentary differentiation caused by tectonic-sedimentary pattern controlled the original sediment types and affected the subsequent diagenetic evolution process.

1 Restricted-evaporative lagoon: The hydrodynamic conditions of this type were relatively weak and the seawater salinity was high because the water circulation was restricted. The lower part developed microcrystal dolomite (Fig. 12(a)), and the upper part developed dolomitic gypsum (Fig. 13(g), (h)). The unique layered component stripes were formed under the influence of frequent transgression and regression, and micrometer-scale argillaceous stripes are distributed in the microcrystal dolomite samples under the microscope. The argillaceous stripes are dark, and the thickness of a single stripe is 0.05–1 mm. The main minerals of the stripes are clay and microcrystal dolomite, which are horizontally laminar or intermittent, with few cracks. The mechanical properties of argillaceous stripes are controlled by the elastic modulus of clay and dolomite minerals. While the anhydrite layer and gypsum-rich stripes in dolomitic gypsum rocks are frequently distributed interactively, with black argillaceous stripes locally. The mechanical properties of gypsum-rich stripes are controlled by the mechanical properties of anhydrite and microcrystal dolomite (major minerals). In addition, because the sediments were in a deep-water environment and were almost not exposed, dissolved pores and cracks were not developed.

2 Mound-shoal: This type is characterized by relatively open water environment, and the hydrodynamic conditions and wave disturbances were strong, resulting in the vertical superposition of granular shoals or microbial mounds. With the continuous evaporation and sedimentation of gypsum salt rocks, high-salinity brine rich in Mg^{2+}, driven by salinity differences, passed through the early sediment area with better porosity and permeability. Microcrystal dolomite was formed under the seepage-reflux dolomitization during this period. Moreover, the mound-shoal was previously exposed several times, resulting in the development of dissolved pores and cracks by atmospheric freshwater leaching transformation. Subsequently, the subsalt strata entered the burial stage, and the temperature and pressure increased. The Mg^{2+}-rich fluid in the overlying Carboniferous clastic rock was released, which provided conditions for burial dolomitization, forming powder or fine-grained dolomite. From the late Indosinian period to the early Yanshanian period, the Upper Paleozoic coal-bearing source rocks entered a peak period of hydrocarbon generation (Yang et al., 2014). The subsalt strata directly contacted with source rocks laterally received hydrocarbon acid fluids, and reservoirs with better porosity and permeability were eroded by fluid flowing along fractures (cracks) and connected pores. As a result, the fractures (cracks) were expanded, and dissolved pores were developed along both sides of the fractures (cracks). The dolomite crystals of reservoir rocks developed in this sedimentary environment are tightly inlaid with each other, and other minerals are basically not load-bearing framework due to their low volume fraction. For this reason, the mechanical properties of samples in the mound-shoal environment are mainly controlled by pore structure (Fig. 13(b), (c)).

3 Platform flat: This type also has a strong evaporation environment, and stromatolite dolomite were developed under the control of microbial vital activities. The compositions of dark layers are mainly microcrystal dolomite, and their mechanical properties are similar to dolomite. While the compositions of bright layers are composed of powder crystal dolomite and

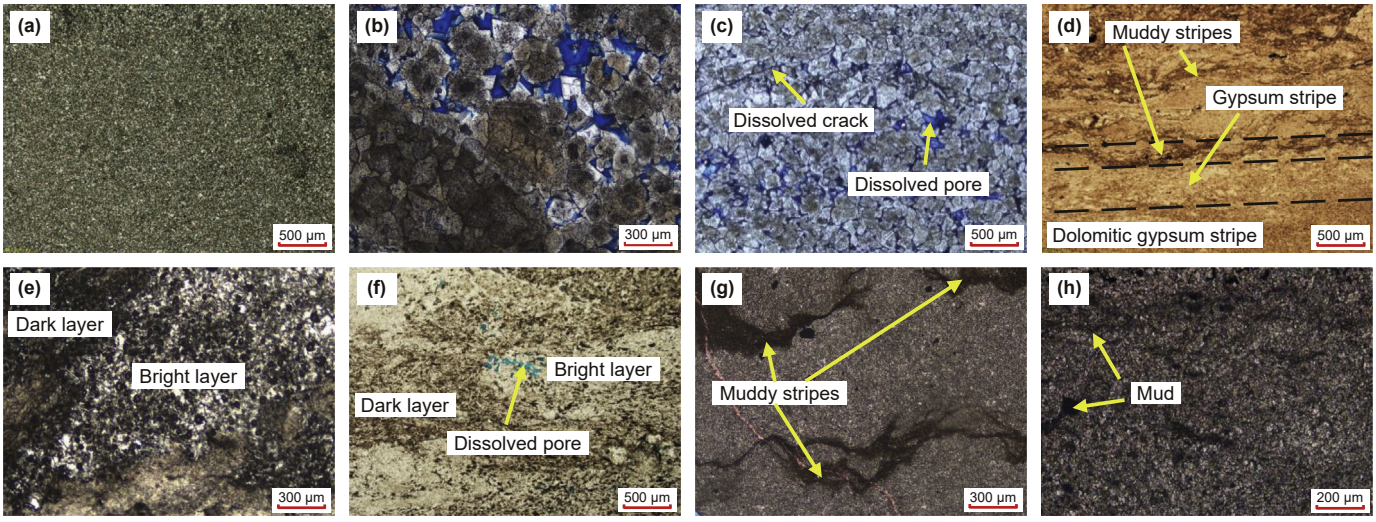

Fig. 13. Rock characteristics of the M_5 subsalt samples in different sedimentary environments. **(a)** Microcrystal dolomite in restricted-evaporate lagoon, intercrystalline pore; **(b)** powder-fine crystalline dolomite in mound-shoal, dissolved pore; **(c)** powder-fine crystalline dolomite in mound-shoal, dissolved pore and dissolved crack; **(d)** dolomitic gypsum in restricted-evaporate lagoon, gypsum stripe and dolomitic gypsum stripe are frequently interbedded, locally intercalated with muddy stripe; **(e)** gypsum dolomite in platform flat, gypsum dolomite layer and dolomite layer interbedded, dissolved pores are seen in samples; **(f)** gypsum dolomite in platform flat, intermittent gypsum dolomite layer; **(g)** argillaceous dolomite in restricted-evaporate lagoon, irregular muddy stripe; **(h)** argillaceous dolomite in restricted-evaporate lagoon, intermittent muddy stripe.

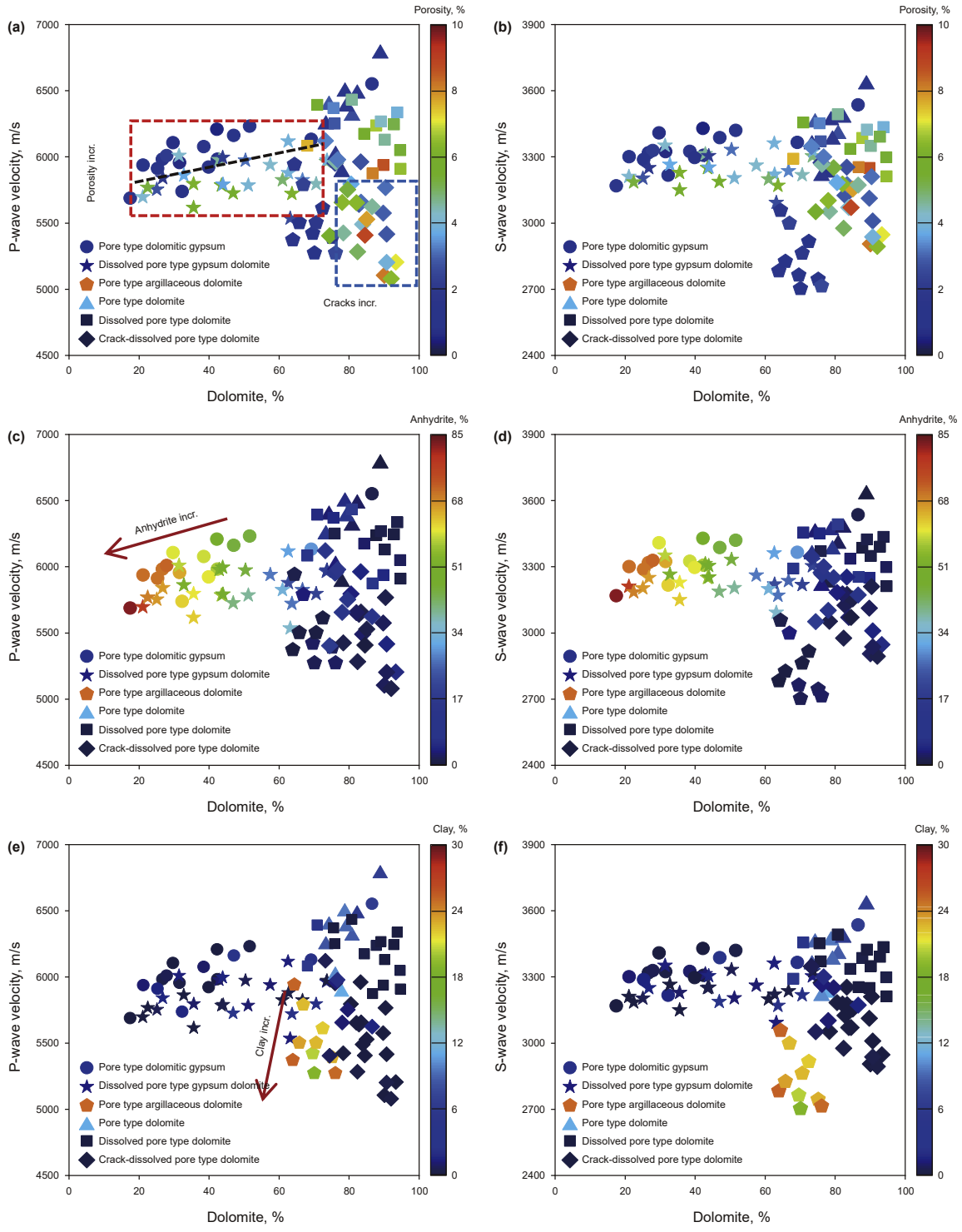

Fig. 14. Variation of V_P and V_S in different types of the M_5 subsalt samples. **(a)**, **(b)** showed effect of dolomite and porosity on V_P and V_S; **(c)**, **(d)** showed effect of dolomite and anhydrite on V_P and V_S; **(e)**, **(f)** showed effect of dolomite and clay on V_P and V_S.

anhydrite (as load-bearing frame), and their mechanical properties are controlled by the elastic moduli of anhydrite crystal and dolomite crystal. Different from the gypsum-rich stripes in the evaporative lagoon, the content of dolomite in bright layers is higher and thus the mechanical properties of bright layers are closer to the elastic modulus of dolomite crystal. Alternatively, there is a greater probability that the platform flat located in the high part of landform was transformed by penecontemporaneous atmospheric fresh water leaching. Many dissolved pores are generated in stromatolite dolomite (Fig. 13(e), (f)), and gypsum karst breccia also indicates that the rocks developed in the platform environment experienced strong atmospheric freshwater leaching and dissolution.

5.2. Links between rock types and rock physics properties

Fig. 14 displays the complex variation trend of V_P and V_S with changes in dolomite content in different types of M_5 subsalt samples. When the dolomite content of samples is less than 55%, the V_P and V_S of pore type dolomitic gypsum and dissolved pore type gypsum dolomite samples increase with increasing dolomite content. Conversely, when dolomite content is higher than 55%, pore-type argillaceous dolomite shows a positive correlation between elastic wave velocities and dolomite content. However, this linear relationship is not found in pore type dolomite, dissolved pore type dolomite, and crack-dissolved pore type dolomite.

To comprehend the variation characteristics of rock acoustic properties, we simplify dolomitic gypsum rock, gypsum dolomite, and argillaceous dolomite into a binary structure unit voxel composed of overlapping stripes of different mineral components (Fig. 15). In the samples with dolomite content less than 55%, lithology transitions from dolomitic gypsum to gypsum dolomite with increasing dolomite content, while anhydrite decreases in strong evaporation environments. The corresponding stripe characteristics primarily show the evolution of anhydrite stripes from continuous to intermittent (Fig. 15(d)). For the elastic wave propagating in the vertical direction, the unit volume element of binary structure is in an equal stress state. Consequently, the equivalent elastic modulus can be simply regarded as the geometric average of the volume ratio of the constituent stripes and their corresponding equivalent elastic modulus, controlled by softer stripes (lower elastic modulus). With continued increase in dolomite content, the continuity of anhydrite stripes diminishes, transitioning from fully stressed continuous stripes to partially stressed intermittent stripes mixed with dolomite. A substantially equal strain state forms in intermittent anhydrite stripes, allowing the equivalent elastic modulus to be considered as the arithmetic average of the corresponding elastic moduli of anhydrite and dolomite. Therefore, the V_P and V_S of samples show an overall trend of increasing with the increase in dolomite. For samples with similar composite minerals, differences in the elastic characteristics of the rock load-bearing frame are minor, and the V_P and V_S are mainly related to porosity. Samples with high porosity (e.g., dissolved pore gypsum dolomite) exhibit lower ultrasonic velocities, resulting in a layered distribution of V_P and V_S based on porosity (as indicated by the red dashed box in Fig. 14(a)). In samples with dolomite content exceeding 55%, lithologies are mostly argillaceous dolomite and dolomite. For argillaceous dolomite, with the increase in dolomite, clay stripes in the corresponding unit volume element evolve from fully stressed continuous stripes to partially stressed intermittent stripes mixed with dolomite stripes. As clay-rich stripes disappear, clays predominantly adhere to dolomite grain boundaries, constituting the

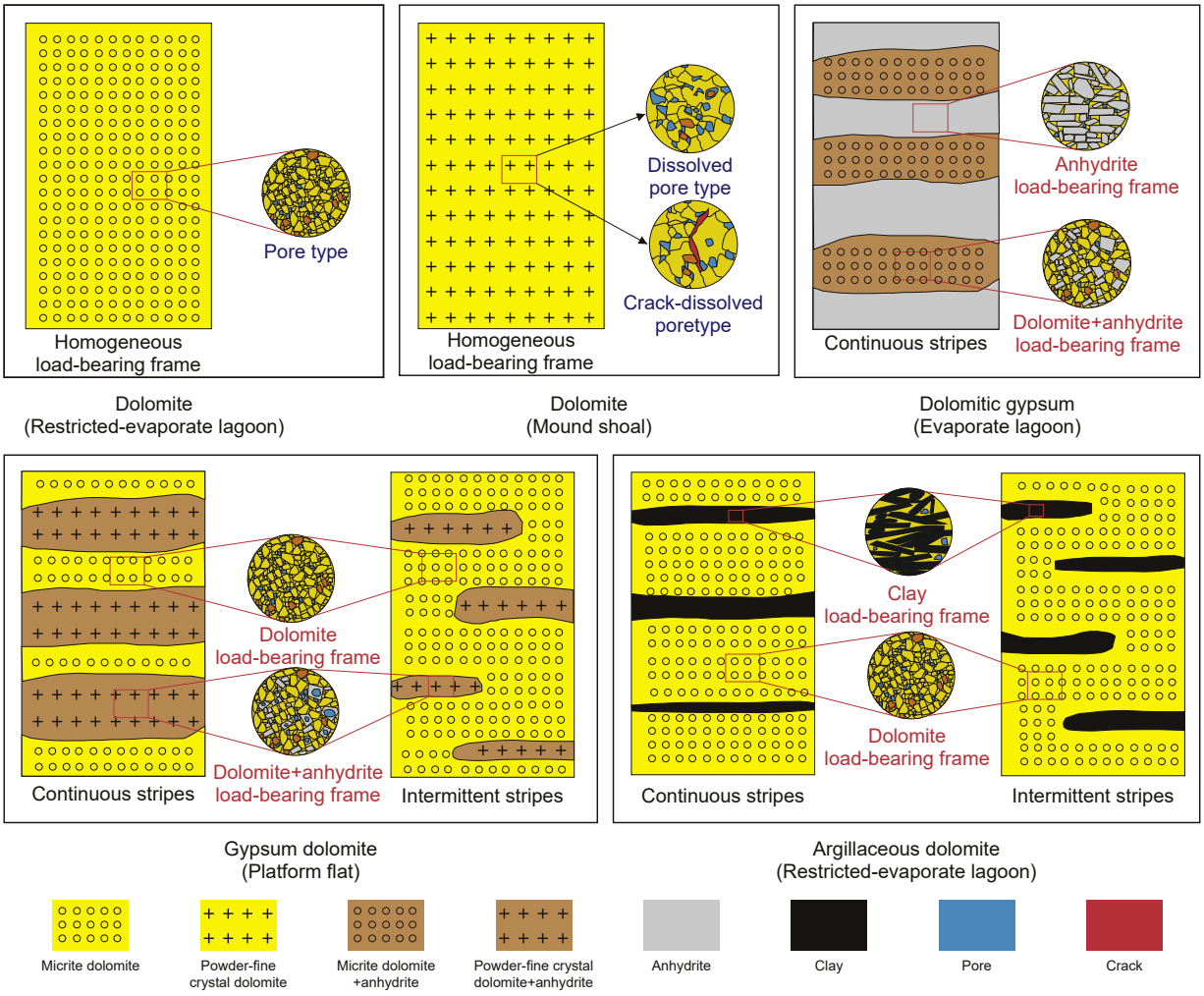

Fig. 15. Schematic diagram of rock characteristics of the M_5 subsalt samples in different sedimentary environments. **(a)** Dolomite in restricted-evaporate lagoon; **(b)** dolomite in mound-shoal; **(c)** dolomitic gypsum in evaporate lagoon; **(d)** gypsum dolomite in platform flat; **(e)** argillaceous dolomite in restricted-evaporate lagoon.

rock load-bearing frame along with dolomite. However, the effect of clay on the equivalent elastic properties is gradually weakened, becoming closer to the elastic properties of dolomite. As a result, the V_P and V_S of argillaceous dolomite samples show an overall increasing trend with the increase in dolomite. Due to the notably lower elastic modulus of clay compared to anhydrite, the ultrasonic velocities of argillaceous dolomite samples are lower than those of gypsum dolomite samples with similar pore structures. Additionally, differences in elastic properties among component stripes (especially continuous stripes) may induce higher velocity anisotropy.

In contrast to dolomitic gypsum, gypsum dolomite, and argillaceous dolomite, the mineral compositions of dolomite samples developed in the mound-shoal environment mainly consist of dolomite, which is no longer the primary factor affecting ultrasonic velocities. Differential changes in V_P and V_S of samples are controlled by the intricate pore structure. Pore types in pore type dolomite samples are singular, predominantly composed of residual inter-crystalline and inter-granular pores with high stiffness (Fig. 15(a)). Furthermore, the equivalent elastic moduli of these samples are less influenced by porosity since their porosity is typically low. Crack-dissolved pore dolomite samples comprise microcracks with lower stiffness and dissolved pores with higher stiffness (Fig. 15(b)). Microcracks with lower stiffness significantly decrease the equivalent elastic modulus of the rock medium, causing a rapid decrease in V_P and V_S with increasing microcracks (as indicated by the blue dashed box in Fig. 14(a)). Dissolved pores have higher stiffness, exerting a lesser effect on the equivalent elastic modulus of rock media compared to microcracks. Nonetheless, the equivalent elastic modulus of mound-shoal dolomite samples also decreases because of the significant development of dissolved pores. Overall, the V_P and V_S of dolomite samples follow the trend: pore type dolomite > dissolved pore type dolomite > crack-dissolved pore type dolomite.

6. Conclusions

The rock characteristics of the M_5 subsalt carbonate in the central Ordos Basin are controlled by various complex geological factors, leading to significant sedimentary differentiation. (1) Argillaceous dolomite and dolomitic gypsum rock predominantly originate from a restricted-evaporative lagoon environment, characterized by small mineral grain sizes and underdeveloped pores. Frequent changes in seawater conditions result in the formation of clay-rich and gypsum-rich stripes. (2) The mound-shoal environment typically features sand-debris dolomite and crystalline dolomite. Affected by intense dissolution and dolomitization, these rocks exhibit high dolomite content and significant development of dissolved pores and cracks. (3) The platform flat areas, situated in higher elevations of the landform, witness the development of stromatolite dolomite and gypsum karst breccia. Mineral components here primarily consist of dolomite and anhydrite. Notably, high salinity seawater and frequent exposure lead to the formation of gypsum-rich stripes and gypsum pores.

The seismic elastic properties of the M_5 subsalt samples are jointly determined by its mineral composition (acting as a load-bearing frame) and pore structure, with porosity playing a secondary role. When clay (clay-rich stripe or clay-type grain boundary), anhydrite (anhydrite-rich stripe or anhydrite crystal tight contact), or dolomite (dolomite crystal dense contact) serve as the load-bearing frame, the ultrasonic velocities (V_P & V_S) of samples with similar pore structure type gradually decrease with increasing clay or anhydrite, and increase with the increasing dolomite. Samples with the same lithology (exhibiting similar grain boundaries or mineral composition stripes) typically show a linear trend in V_P and V_S. Other elastic properties, such as P-wave impedance and Poisson's ratio, are also influenced by microstructure. Specifically, microcracks with lower stiffness significantly reduce the P-wave impedance and Poisson's ratio of dry samples. Upon saturation with brine, microcracks cause a significant increase in Poisson's ratio, while high-stiffness pores or dissolved pores have minimal effect on Poisson's ratio.

CRediT authorship contribution statement

Jia-Qing Wang: Writing – original draft, Formal analysis, Conceptualization. **Ji-Xin Deng:** Writing – review & editing, Funding acquisition. **Zhong-Hua Xu:** Data curation. **Hui Xia:** Data curation. **Long-long Yan:** Data curation.

Declaration of competing interest

The authors declare that they have no known competing financial interests or personal relationships that could have appeared to influence the work reported in this paper.

Acknowledgement

This work is supported by the National Natural Science Foundation of China (41774136, 42474149), data will be available on request. There are no conflicts of interest.

Appendix A. Supplementary data

Supplementary data to this article can be found online at https://doi.org/10.1016/j.petsci.2024.05.024

References

Abdlmutalib, A., Abdullatif, O., Abdelkarim, A., et al., 2019. Factors influencing acoustic properties of carbonate rocks: examples from middle Jurassic carbonates, Central Saudi Arabia. J. Afr. Earth Sci. 150 (FEB), 767–782. https://doi.org/10.1016/j.jafrearsci.2018.10.005.

Berryman, J.G., 1992. Single-scattering approximations for coefficients in Biot's equations of poroelasticity. J. Acoust. Soc. Am. 91 (2), 551–571. https://doi.org/10.1121/1.402518.

Brigaud, B., Vincent, B., Durlet, C., et al., 2010. Acoustic properties of ancient shallow-marine carbonates: effects of depositional environments and diagenetic processes (Middle Jurassic, Paris Basin, France). J. Sediment. Res. 80 (9), 791–807. https://doi.org/10.2110/jsr.2010.071.

Chen, A.Q., Yang, S., Xu, S., et al., 2019. Sedimentary model of marine evaporites and implications for potash deposits exploration in China. Carbonates Evaporites 34 (1), 83–99. https://doi.org/10.1007/s13146-018-0443-0.

Ehrenberg, S.N., 2006. Porosity destruction in carbonate platforms. J. Petrol. Geol. 29 (1), 41–52. https://doi.org/10.1111/j.1747-5457.2006.00041.x.

Fang, S.X., He, J., Hou, F.H., 2009. Reservoirs pore space types and evolution $M5^5$ to $M5^1$ submembers of Majiagou Formation of Middle Ordovician in central gasfield area of Ordos Basin. Acta Petrol. Sin. 25 (10), 2425–2441 (in Chinese).

Feng, Z.Z., Bao, Z.D., 1999. Lithofacies paleogeography of Majiagou age of ordovician in Ordos Basin. Acta Sedimentol. Sin. 17 (1), 1–8 (in Chinese).

Fu, S.Y., Zhang, C.G., Chen, H.D., et al., 2019. Characteristics, formation and evolution of pre-salt dolomite reservoirs in the fifth member of the Ordovician Majiagou Formation, mid-east Ordos Basin, NW China. Petrol. Explor. Dev. 46 (6), 1087–1098. https://doi.org/10.11698/PED.2019.06.07.

Hornby, E.B., 1998. Experimental laboratory determination of the dynamic elastic properties of wet, drained shales. J. Geophys. Res. 103 (B12), 945–964. https://doi.org/10.1029/97JB02380.

He, J., Fang, S.X., Hou, F.H., et al., 2009. Characteristics of karst reservoirs in the middle ordovician Majiagou Formation of gas field in the central Ordos Basin. Oil Gas Geol. 3, 350–356 (in Chinese). doi: JournalArticle/5af4923ec095d718d81b4a36.

He, J., Fang, S.X., Hou, F.H., 2013. Vertical zonation of weathered crust ancient karst and the reservoir evaluation and prediction—a case study of $M5^5$-$M5^1$ submembers of Majiagou Formation in gas fields, central Ordos Basin, NW China. Petrol. Explor. Dev. 40 (5), 534–542. https://doi.org/10.11698/PED.2013.05.04.

Huang, Z.L., Liu, Y., Wu, C.Y., et al., 2014. Characteristics of hydrocarbon accumulation in the middle and lower sections of middle assemblages of lower ordovician Majiagou member-5, Ordos Basin. Mar. Petrol. Geol. 19 (3), 57–65. https://doi.org/10.3969/j.issn.1672-9854.2014.03.008 (in Chinese).

Kenter, J.A.M., Podladchikov, F.F., Reinders, M., 1997. Parameters controlling sonic velocities in a mixed carbonate-siliciclastics Permian shelf-margin (upper San Andres formation, Last Chance Canyon, New Mexico). Geophysics 62 (2), 505–520. https://doi.org/10.1190/1.1444161.

Li, J.J., Song, Z.W., Zhang, C.L., et al., 2022. Study of the gas sources of the ordovician gas reservoir in the central-eastern Ordos Basin. Petrol. Sci. 19 (3), 949–962. https://doi.org/10.1016/j.petsci.2021.12.023.

Ma, Y.S., He, D.F., Cai, X.Y., et al., 2017. Distribution and fundamental science questions for petroleum geology of marine carbonate in China. Acta Petrol. Sin. 33 (4), 1007–1020 (in Chinese).

Mavko, G., Mukerji, J., Dvorkin, J., 2009. In: The Rock Physics Handbook: Tools for Seismic Analysis of Porous Media, second ed. Cambridge University Press, New York.

Pickett, G.R., 1963. Acoustic Character logs and their applications in formation evaluation. J. Petrol. Technol. 15 (6), 659–667. https://doi.org/10.2118/452-PA.

Sharifi, J., 2022. Intelligent pore type characterization: improved theory for rock physics modelling. Geophys. Prospect. 70, 921–937. https://doi.org/10.1111/1365-2478.13204.

Teillet, T., Fournier, F., Zhao, L., et al., 2021. Geophysical pore type inversion in carbonate reservoir: integration of cores, well logs, and seismic data (Yadana field, offshore Myanmar). Geophysics 86 (3), 1–69. https://doi.org/10.1190/geo2020-0486.1.

Xi, S.L., Xiong, Y., Liu, X.Y., et al., 2017. Sedimentary environment and sea level change of the subsalt interval of Member 5 of Ordovician Majiagou Formation in central Ordos Basin. J. Palaegeogr. 19 (5), 773–790. https://doi.org/10.7605/gdlxb.2017.05.061 (in Chinese).

Xi, S.L., Liu, X.S., Ren, J.F., et al., 2023. New understanding of hydrocarbon accumulation and exploration potential in risk exploration field in Ordos Basin. Chin. Petrol. Explor. 28 (3), 34–48. https://doi.org/10.3969/j.issn.1672-7703.2023.03.004 (in Chinese).

Xia, M.J., Zheng, Z.B., Dai, J.X., et al., 2007. Ordovician under-salt reservoirs and forming conditions of gas pools in eastern Ordos Basin. Nat. Gas Geosci. 20 (4), 204–208. https://doi.org/10.3969/j.issn.1672-1926.2007.02.009 (in Chinese).

Xia, M.J., Zeng, D.Q., Deng, R.J., et al., 2009. Reef and shallow facies and reservoir characteristics in Changxing Formation platform margin, Puguang Gas Field. Nat. Gas Geosci. 20 (4), 549–562 (in Chinese).

Xiong, Y., Tan, X.C., Zuo, Z.F., et al., 2019. Middle Ordovician multi- stage penecontemporaneous karstification in North China: implications for reservoir genesis and sea level fluctuations. J. Asian Earth Sci. 183, 1–14. https://doi.org/10.1016/j.jseaes.2019.103969.

Yang, H., Bao, H.P., Ma, Z.R., 2014. Reservoir-forming by lateral supply of hydrocarbon: a new understanding of the formation of Ordovician gas reservoirs under gypsolyte in the Ordos Basin. Nat. Gas. Ind. 34 (9), 19–26. https://doi.org/10.3787/J.ISSN.1000-0976.2014.04.003 (in Chinese).

Yao, J.L., Bao, H.P., Ren, J.F., et al., 2015. Exploration of ordovician subsalt natural gas reservoirs in Ordos Basin. Chin. Petrol. Explor. 20 (3), 1–12. https://doi.org/10.3969/j.issn.1672-7703.2015.03.001 (in Chinese).

Yao, J.L., Wang, C.C., Chen, J.P., et al., 2016. Distribution characteristics of subsalt carbonate source rocks in Majiagou Formation, Ordos Basin. Nat. Gas Geosci. 27 (12), 2115–2126. https://doi.org/10.11764/j.issn.1672-1926.2016.12.2115 (in Chinese).

Yin, H., 1992. Acoustic Velocity and Attenuation of Rocks: Isotropy, Intrinsic Anisotropy, and Stress Induced Anisotropy. Ph.D. Thesis, Stanford University, San Francisco, America, pp. 179–193.

Yu, Z., Ding, Z.C., Wang, L.H., et al., 2018. Main factors controlling formation of dolomite reservoir underlying gypsum-salt layer in the 5th member of Ordovician Majiagou Formation, Ordos Basin. Oil Gas Geol. 39 (6), 1213–1224. https://doi.org/10.11743/ogg20180611 (in Chinese).

Zhao, L.X., Nasser, M., Han, D.H., 2013. Quantitative geophysical pore-type characterization and its geological implication in carbonate reservoirs. Geophys. Prospect. 61 (4), 827–841. https://doi.org/10.1111/1365-2478.12043.

Zhong, S.K., Tan, X.V., Hu, G., et al., 2022. Control of paleogeographic pattern on sedimentary differentiation of evaporite-carbonate symbiotic system: a case study of the sixth sub-member of Ordovician Majiagou Formation M5 Member in central-eastern Ordos Basin, NW China. Petrol. Explor. Dev. 49 (4), 728–740. https://doi.org/10.11698/PED.20220077.

Zhou, J.G., Xu, C.C., Yao, G.S., 2015. Genesis and evolution of lower cambrian longwangmiao formation reservoirs, Sichuan Basin, SW China. Petrol. Explor. Dev. 42 (2), 158–166. https://doi.org/10.11698/PED.2015.02.04.

Zou, C.N., Xie, Z.Y., Li, J., et al., 2023. Differences and main controlling factors of large-scale gas accumulations in typical giant carbonate gas fields: a case study on Anyue gas field in the Sichuan Basin and Jingbian gas field in the Ordos Basin. Oil Gas Geol. 44 (1), 1–15. https://doi.org/10.11743/ogg20230101 (in Chinese).